Journal of the Korean Electrochemical Society
Vol. 22, No. 4, 2019, 172-176
https://doi.org/10.5229/JKES.2019.22.4.172

Research Paper
pISSN 1229-1935
eISSN 2288-9000

Designing of a Novel Core-Shell-Structured Co-free Cathode Material with Enhanced Thermal and Structural Stability for Lithium Ion Batteries

Ji-Woong Shin, Yun-Chae Nam, and Jong-Tae Son*

Department of Nano Polymer Science & Engineering, Korea National University of Transportation, Chungju, Chungbuk 27469, Korea

(Received October 21, 2019 : Revised November 25, 2019 : Accepted November 27, 2019)

Abstract : The first commercialized cathode material, $LiCoO_2$, suffers from disadvantages such as high cost and toxicity and also possesses safety problems. The nickel-rich $LiNi_{0.9}Mn_{0.1}O_2$ cathode material, used as an alternative to $LiCoO_2$, has highly reversible capacity and high energy density. So, the nickel-rich $LiNi_{0.9}Mn_{0.1}O_2$ cathode material is widely used as an alternative to $LiCoO_2$ due to its highly reversible capacity and high energy density. However, $LiNi_{0.9}Mn_{0.1}O_2$ has several disadvantages as well, such as poor cycle performance and poor thermal instability. To address these problems, we synthesized a new material, $LiNi_{0.5}Mn_{0.5}O_2$, as a shell on the surface of a core to suppress the surface degradation. The new material showed high structural and thermal stabilities and could also maintain a high capacity. The capacity retention of the core-shell cathode (87.7%) was better than that of the core cathode (76.9%) after 50 cycles. Analysis using differential scanning calorimetry revealed that the heat generation in the core-shell cathode (65.9 Jg^{-1}) was lower than that in the core cathode (559.7 Jg^{-1}).

Keywords : Cobalt-Free, Core-Shell Structure, Cathode Material

1. Introduction

Lithium ion batteries are widely applied in portable electronic devices at present due to their high energy densities, low self-discharge, and tiny memory effect.[1,2] The $LiCoO_2$ has been the most widely used cathode material because of its stable electrochemical cycling and ease of production. However, $LiCoO_2$ cathode material suffers from the disadvantages of high cost and toxicity and also possesses safety problems.[3-6] Cobalt free $LiNi_{0.9}Mn_{0.1}O_2$ cathode material has been proposed as an alternative to $LiCoO_2$ because of its relatively low material cost, structural similarity, and higher discharge capacity. However, it is difficult to maintain the high capacity because its structure is prone to degradation and is accompanied by the release of oxygen, which causes a violent exothermic reaction at a deeply charged state.[7] The layered $LiNi_{0.9}Mn_{0.1}O_2$ cathode material too has some disadvantages. For instance, it has a poor cycle performance because the oxidation state of nickel changes from +2 to +4, and Ni^{4+} being unstable, reacts with the electrolyte and decreases the capacity drastically.[8] It is possible to create a functional layer (or shell) on the surface of the inorganic particles (core); materials with such a structure are called the core-shell materials. These materials have attracted a great deal of interest because of their improved physical and chemical properties over their single-component counterparts.[9,10] Ohzuku and Makimura introduced a $LiNi_{0.5}Mn_{0.5}O_2$ cathode material which was different from $LiNiO_2$. The average oxidation state of nickel in this material was +3, and the formal charges of nickel and manganese were +2 and +4, respectively.[11-13] Since tetravalent manganese is electrochemically inactive, it provides significant structural stability to the material and results in a

*E-mail: jt1234@ut.ac.kr

simple topotactic reaction maintaining the hexagonal phase during electrochemical cycling, even at a high voltage cutoff limit of 4.6 V.[14-17] Due to its improved structural stability, the onset of the exothermic reaction in $LiNi_{0.5}Mn_{0.5}O_2$ is usually at a temperature as high as 280°C, and the heat generation at this temperature is less than that in $LiNi_{0.9}Mn_{0.1}O_2$.[18,19] Thus, taking advantages of both high capacity and high thermal stability, we have designed a spherical core-shell material with $LiNi_{0.9}Mn_{0.1}O_2$ as the core and $LiNi_{0.5}Mn_{0.5}O_2$ as the shell. The core delivers a high capacity of around 200 $mAhg^{-1}$, while the shell provides significant structural and thermal stability upon electrochemical cycling. The electrochemical properties and thermal stabilities of the core $LiNi_{0.9}Mn_{0.1}O_2$ and the $Li[(Ni_{0.9}Mn_{0.1}O_2)_{1-x}(Ni_{0.5}Mn_{0.5})_x]O_2$ core-shell cathode materials were investigated using electrochemical testing and differential scanning calorimetry (DSC).

2. Experiment Details

The precursor, $Ni_{0.9}Mn_{0.1}(OH)_2$, and the core-shell material, $[(Ni_{0.9}Mn_{0.1})_{1-x}(Ni_{0.5}Mn_{0.5})_x](OH)_2$, were synthesized via co-precipitation. Aqueous solutions of 1 M $NiSO_4 \cdot 6H_2O$ and 1 M $MnSO_4 \cdot H_2O$ were pumped into a 4 L tank reactor with continuous stirring under a N_2 atmosphere to generate the precursor. At the same time, NaOH (2 M) and NH_4OH solution were separately fed into the reactor. The co-precipitation under vigorous stirring resulted in the formation of spherical particles. In order to construct the core-shell material with a composition of $[(Ni_{0.9}Mn_{0.1})_{1-x}(Ni_{0.5}Mn_{0.5})_x](OH)_2$, the prepared precursor, $Ni_{0.9}Mn_{0.1}(OH)_2$, was continuously mixed with the solution containing the metal compounds. The resulting $Ni_{0.9}Mn_{0.1}(OH)_2$, $[(Ni_{0.9}Mn_{0.1})_{1-x}(Ni_{0.5}Mn_{0.5})_x](OH)_2$ particles were filtered, washed, and then dried in a vacuum oven at 120°C for 24 h. The $Li[Ni_{0.9}Mn_{0.1}]O_2$ and $Li[(Ni_{0.9}Mn_{0.1})_{1-x}(Ni_{0.5}Mn_{0.5})_x]O_2$ samples were calcined with the precursor and LiOH at 750°C for 10 h in an O_2 atmosphere. X-ray diffraction (XRD) patterns for the cathodes were obtained using a Siemens D X-ray diffractometer equipped with Cu Kα radiation (λ = 1.54068 Å) in the 2θ range from 10 to 70°. The morphology of the powder was observed using scanning electron microscopy (SEM). The cathode was fabricated by blending the active material, super P carbon, and binder in 8:1:1 ratio in *N*-methyl-2-pyrrolidone. The mixed slurry was cast uniformly on a thin Al foil and dried in vacuum for 12 h at 120°C. The electrochemical performance was tested using a CR2032 coin-type cell, with lithium-metal foil as the anode. A polypropylene microporous film was used as the separator. $LiPF_6$ (1 M) in a 3:7 (v/v) mixture of ethylene carbonate (EC) and diethyl carbonate (DEC) was used as the electrolyte. The cells were assembled in an argon-filled glove box. The electrochemical performances were tested between 2.7 and 4.5 V.

3. Results and Discussion

Fig. 1 shows the SEM images of the core, core-shell, and shell precursors and their corresponding cathode materials. The figure also demonstrates the cross-sectional SEM images and EDS line profile of the core–shell cathode material. The $Ni_{0.9}Mn_{0.1}(OH)_2$ core precursor was synthesized by co-precipitation and the $Ni_{0.5}Mn_{0.5}(OH)_2$ shell layer was synthesized by changing the composition of the metal solution in the co-precipitation reactor. The diameter of the spherical core and the thickness of the shell layer were ~5 and ~1 μm, respectively. The EDS line profile analysis of the core-shell material shows nearly the intended composition. The composition of the core cathode material was quite close to the designed composition. The nickel and manganese contents gradually changed from line size 0-1 μm and 5-6 μm. The image of the cross-section confirms that the core-shell cathode material was distinctly divided at the interface of the core and shell, suggesting that the core-shell structure had been successfully synthesized.

Fig. 2 shows the XRD patterns of the synthesized core, core-shell, and shell cathode materials. The XRD patterns of all the materials can be indexed to the α-$NaFeO_2$ structure (space group *R*-3*m*). The *I*(003)/*I*(104) ratios of the core, core-shell, and shell materials were 1.0794, 1.0080, and 1.0025, respectively. The cation mixing, represented as the amount of Ni^{2+} in lithium layer,

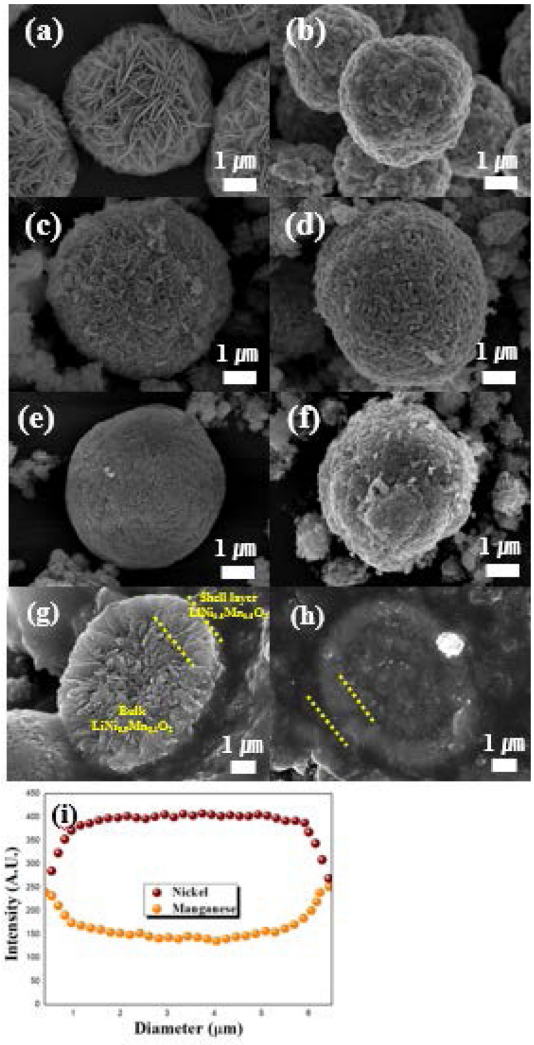

Fig. 1. SEM images of the (a) core precursor, (b) core cathode material, (c) core-shell precursor, (d) core-shell cathode material, (e) shell precursor, (f) shell cathode material, (g), (h) cross-section of the core-shell cathode material and (i) EDS line profile of the core shell cathode material.

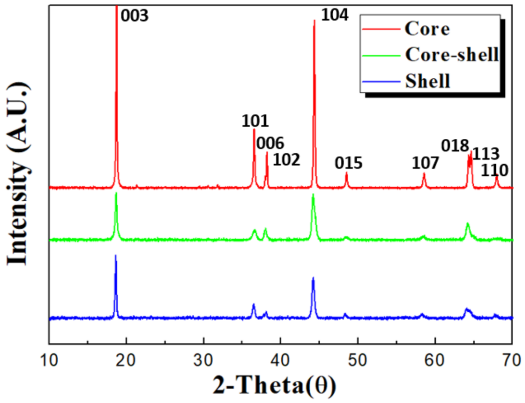

	a (Å)	c (Å)	$I_{(003)} / I_{(104)}$
Bare	2.8787 (±0.0004)	14.2150 (±0.0012)	1.0794
Core-shell	2.8635 (±0.0008)	14.0589 (±0.0015)	1.0080
Shell	2.8611 (±0.0009)	14.0324 (±0.0013)	1.0025

Fig. 2. XRD pattern of the core, core-shell, and shell cathode materials.

increased with increasing manganese content. Since the total amount of Ni^{2+} increases with increasing Mn content in $Li(Ni^{2+}_{x}Ni^{3+}_{1-2x}Mn^{4+}_{x})O_2$, the Ni^{2+} content in the lithium layer would also increase.[20]

Fig. 3 (a) shows the initial charge/discharge capacity curves of the core, core-shell, and shell cells in the cutoff range of 2.7 to 4.5 V at 0.1 C (27.5 mAg^{-1}). The core electrode delivered a high discharge capacity of 191.4 $mAhg^{-1}$, while the core-shell and shell electrode exhibited slightly lower capacities of 174.4 and 149.8 $mAhg^{-1}$. This can be attributed to the lower nickel fraction in the outer layer. To verify the Li-extraction-induced phase transitions during cycling, the dQ/dV profiles of both the cathode materials were obtained by differentiating the charge/discharge curves. The dQ/dV profiles in Fig. 3(b) show a series of phase transitions similar to those observed in Ni-rich cathode materials. The H2 ↔ H3 phase transition above 4.0 V can be attributed to the abrupt lattice shrinkage/expansion of both the core and core–shell electrodes. This H2 ↔ H3 phase transition in the core and core-shell cathode materials is likely to be responsible for the structural degradation. The precursor and cathode of the core-shell and shell materials cause capacity loss because the surface of the secondary particles is smooth and denser which makes the lithium ions unable to escape. Thus, in the dQ/dV plot of the first cycle, the core-shell and shell material did not show H2 ↔ H3 phase transition. The relative intensities of the H2 ↔ H3 phase transition peaks in the

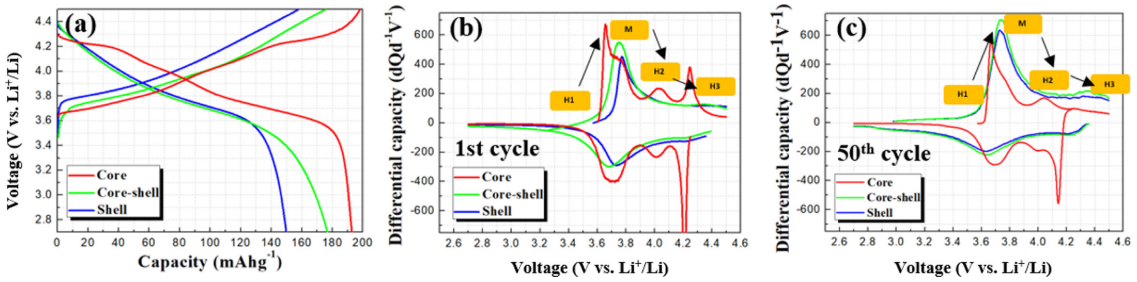

Fig. 3. (a) Initial charge/discharge curves and (b), (c) differential capacity (d*Q*/d*V*) curves of the core, core-shell, and shell cathode materials.

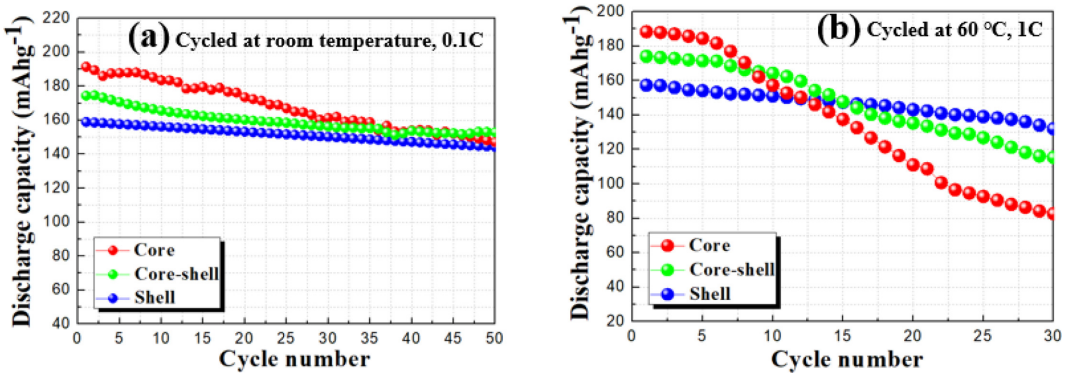

Fig. 4. Cycling performances of the core, core-shell, and shell cathode materials at (a) 0.1 C at room temperature and (b) 1 C at 60°C.

d*Q*/d*V* profiles of the core, core-shell, and shell cathode materials suggest that the detrimental phase transition was substantially suppressed in the core-shell cathode material.

Figs. 4(a) and (b) show the cycling performances of the synthesized core, core-shell, and shell electrodes at room temperature and 60°C, at current densities of 27.5 and 275 mAg^{-1}, respectively. The capacity retention of the core and core-shell electrodes were 76.9% and 87.7%, respectively, at room temperature after 50 cycles, suggesting that the capacity retention of the core-shell electrode was much higher than that of the core electrode. The capacity retention of the shell electrode was 90.7%. Even at high temperature, the capacity retention of the core-shell cathode material was 66.3% after 30 cycles, which outperformed that of the core cathode material (43.9% capacity retention). The poor cycling performance of Ni-rich cathode material could originate from the formation of impurity Li_x-$Ni_{1-x}O$ phase from $Li_{1-\delta}[Ni_{1-x}M_x]O_2$ due to the presence of highly reactive and unstable Ni^{4+}, which can increase the interfacial impedance and thus decrease the cycle life of the cell. We believe that the decreased Ni concentration and the increased Mn concentration in the outer shell layer play an important role in stabilizing the near-surface region of the core-shell cathode material and reduce its reactivity with electrolyte.[21,22]

Fig. 5 shows the DSC profiles of the core and core-shell materials charged to 4.5 V in the presence of 1 M $LiPF_6$/EC:DEC electrolyte. The onset temperature for the exothermic reaction peak in the DSC thermogram of the core material is 227.9°C; the corresponding temperature for the core-shell material is 244.7°C. This indicates the reduced heat generation in the core-shell material as compared with that of the core material.

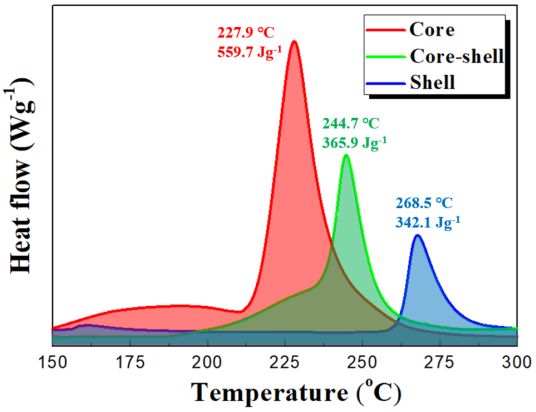

Fig. 5. DSC traces of the core, core-shell, and shell cathode materials charged to 4.5 V.

4. Conclusions

The electrochemical and thermal properties of the $LiNi_{0.9}Mn_{0.1}O_2$ core and $Li[(Ni_{0.9}Mn_{0.1}O_2)_{1-x}(Ni_{0.5}Mn_{0.5})_x]O_2$ core-shell particles synthesized by co-precipitation were characterized. The $LiNi_{0.9}Mn_{0.1}O_2$ core electrode delivered a high capacity, while the $LiNi_{0.5}Mn_{0.5}O_2$ shell provided high thermal and structural stability. In lithium ion cells, the core-shell electrode exhibited an excellent cyclability with a capacity retention of 87.7% after 50 cycles, while the core electrode exhibited a capacity retention of only 76.9% for the same number of cycles in the same cells. In the 50 cycle dQ / dV plot, the phase transition peaks of the core-shell and shell material was significantly reduced compared to the core material. As a result, the amount of electrochemically inactive Mn^{4+} increases, confirming that the crystal structure has stabilized. Also, the cycle performance at room temperature and high temperature were excellent. The thermal stability of the fully charged core-shell electrode was found to be considerably better than the core electrode. We propose that the core-shell-structured cobalt-free cathode material having high capacity and high thermal and structural stability can be suitably used in rechargeable lithium ion batteries.

Acknowledgment

This study was supported by the financial resources granted by the Ministry of Trade Program on Industry & Energy, Republic of Korea (Grant No. G02N03620000901) and National Research Foundation of Korea (NRF) grant funded by the Korea government (MIST) (No.2019R1F1A1057220)

References

1. T. Sasaki, Y. Ukyo, and P. Novaak, *J. Nat. Mater.*, **12**, 569 (2013).
2. Y. P. Zhang, E. Q. Liang, J. X. Wang, B. J. Yu, C. Y. Wang, and M. W. Li, *Int. J. Electrochem. Sci.*, **12**, 9051 (2017).
3. M. S. Islam, R. A. Davies, and J. D. Gale, *Chem. Mater.*, **15**, 4280 (2003).
4. Jeffery W. and Fergus, *J. Power Source*, **195**, 939 (2010).
5. D. Li, C. Yuan, J. Dong, Z. Peng, and Y. Zhou, *J. Solid State Chem.*, **12**, 323 (2008).
6. D. Gao, Y. Li, X. Lai, J. Bi and D. Lin, *J. Alloys Comp.*, **509**, 697 (2011).
7. H. Arai, S. Okada, Y. Sakurai, and Yamaki, *J. Solid State Ionics*, **109**, 295 (1998).
8. F. L. Liu, S. Zhang, C. Deng, Q. Wu, M. Zhang, F. L. Meng, H. Gao, and Y. H. Sun, *J. Electrochem. Soc.*, **159**, 1591 (2012).
9. I.L. Radtchenko, G.B. Sukhorukov, N. Gaponik, A. Kornowski, A.L. Rogach, and H. Mohwald, *Adv. Mater.*, **13**, 1684 (2001).
10. Y. K. Sun, S. T. Myung, B. C. Park, and K. Amine, *Chem. Mater.*, **18**, 5159 (2006).
11. T. Ohzuku and Y. Makimura, *Chem. Lett.*, **30**, 744 (2001).
12. W. Ahn, S. N. Lim, K. N. Jung, S. H. Yeon, K. B. Kim, H. S. Song, and K. H. Shin, *J. Alloys Comp.*, **609**, 143 (2014).
13. Z. Lu, L.Y. Beaulieu, R.A. Donaberger, C.L. Thomas, and J.R. Dahna, *J. Electrochem. Soc.*, **149**, 778 (2002).
14. X.Q. Yang, J. McBreen, S.W. Yoon, and C.P. Grey, *Electrochem. Commun.*, **4**, 649, (2002).
15. S.T. Myung, S. Komaba, K. Hosoya, N. Hirosaki, U. Miura, and N. Kumagai, *Chem. Mater.*, **17**, 2427 (2005).
16. Z. Lu, L.Y. Beaulieu, R.A. Donaberger, C.L. Thomas, and J.R. Dahn, *J. Electrochem. Soc.*, **149**, 778 (2002).
17. Y. K. Sun, S. T. Myung, M. H. Kim, J. Prakash, and K. Amine, *J. Am. Chem. Soc.*, **127**, 13411 (2005).
18. S.H. Kang, J. Kim, M.E. Stoll, D. Abraham, Y.K. Sun, and K. Amine, *J. Power Source*, **112**, 41 (2002).
19. S. Jouanneau, D.D. MacNeil, Z. Lu, S.D. Beattie, G. Murphy, and J.R. Dahn, *J. Electrochem. Soc.*, **150**, 1299 (2003).
20. Y. K. Sun, D. J. Lee, Y. J. Lee, Z. Chen, and S. T. Myung, *ACS Appl. Mater Interfaces*, **5**, 11434 (2013).
21. Y. K. Sun, D. H. Kim, C. S. Yoon, S. T. Myung, J. Prakash and K. Amine, *Adv. Funct. Mater.*, **20**, 485 (2010).
22. Y. K. Sun, B. R. Lee, H. J. Noh, H. Wu, S. T. Myung and K. Amine, *J. Mater. Chem.*, **21**, 10108 (2011)